THE JOURNAL OF PHYSICAL CHEMISTRY C
A JOURNAL OF THE AMERICAN CHEMICAL SOCIETY

pubs.acs.org/JPCC

Article

Density Functional Theory Study and Photocatalytic Activity of ZnO/N-Doped TiO_2 Heterojunctions

Wanda Navarra,[‖] Ida Ritacco,[‖] Olga Sacco,[‖] Lucia Caporaso,* Matteo Farnesi Camellone, Vincenzo Venditto,* and Vincenzo Vaiano

Cite This: *J. Phys. Chem. C* 2022, 126, 7000–7011

Read Online

ACCESS | Metrics & More | Article Recommendations | Supporting Information

ABSTRACT: The beneficial effects on ZnO and TiO_2 photocatalytic activity resulting from a suitable combination of doping and heterojunctions were proposed and investigated by a synergistic experimental and theoretical study. In detail, the ZnO/N-doped TiO_2 heterojunction was synthesized and tested in the photocatalytic degradation of atrazine under UV and visible light. Wide-angle X-ray diffraction (WAXD) analysis reveals the presence of both ZnO and TiO_2 crystalline phases in the heterojunction. UV−vis DRS analysis shows that the simultaneous presence of ZnO and N-doped TiO_2 in the heterojunction results in a slight increase in the band gap value in the UV region , while the shoulder in the visible region typically of bare N-doped TiO_2 is preserved. On the basis of these experimental observations, density functional theory (DFT) calculations were carried out to model both the N-doped TiO_2 structure and to rationalize the experimental decrease in the band gap energy. The DFT modeling of band alignment of the ZnO/N-doped TiO_2 heterojunction allowed us to define the "minimal band gap" (MBG), corresponding to the interface gap, which resulted in smaller band gap energy than the two separate semiconductor band gaps. Furthermore, the DFT modeling of the electronic structure of N-doped TiO_2 predicted the existence of additional energy levels between the TiO_2 valence and conduction bands, which allowed us to justify the activity of the heterojunction under visible light irradiation. Photocatalytic tests showed that the ZnO/N-doped TiO_2 heterojunction performance was better than that of both N-doped TiO_2 and ZnO alone, allowing us to achieve almost complete atrazine degradation under UV light irradiation, whereas 24% of atrazine degradation was achieved after 180 min of visible light irradiation. Finally, the photocatalytic results achieved by using scavenger molecules for reactive oxygen species showed that •OH and $\cdot O_2^-$ are both reactive species in atrazine photocatalytic degradation under UV irradiation, while •OH is responsible for the photocatalytic processes under visible irradiation. DFT modeling, validated by these results, finally allowed us to define a model of the band alignment and photogenerated charge-transfer mechanism for the ZnO/N-doped TiO_2 heterojunction.

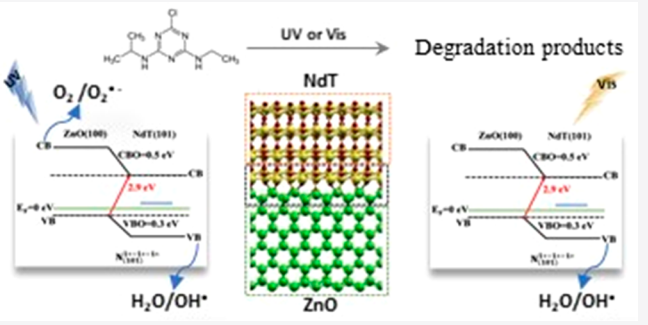

Downloaded via SISSA on April 28, 2022 at 08:17:55 (UTC).
See https://pubs.acs.org/sharingguidelines for options on how to legitimately share published articles.

1. INTRODUCTION

In the last years, search for new materials with improved optoelectronic properties,[1,2] as well as new ways to efficiently use solar energy, the most abundant energy source on earth, has attracted increasing interest.[3] In the field of environmental pollutant degradation, heterogeneous photocatalysis has received great attention because it is a sustainable water remediation process that can be carried out in the presence of sunlight.[4] Semiconductor-based materials are the most studied catalysts in photocatalytic processes. Due to their electronic structure including an electron-filled valence band (VB) and an empty conduction band (CB), in the presence of an electromagnetic radiation with energy equal to or greater than band gap (E_g), the excited electrons from the VB are injected into the CB, thus leaving a reactive hole on the VB. Therefore, h^+ left in the VB and e^- introduced into the CB have oxidative and reducing capacities, respectively. Indeed, if the photogenerated e^- and h^+ have suitable potential, they could react with H_2O and O_2, respectively, to produce strong oxidative radicals (hydroxyl radicals and superoxides) capable of promoting the degradation of organic pollutants into harmless inorganic materials.[5] However, still many challenges need to be overcome to obtain viable photocatalysts for the actual application. The major challenge is to find suitable semiconductors having CB, VB, and band gap energies, which make the best use of solar energy and maximize the generation of reactive oxygen species (ROS) along with extending the e^-/

Received: January 8, 2022
Revised: March 31, 2022
Published: April 13, 2022

© 2022 American Chemical Society

https://doi.org/10.1021/acs.jpcc.2c00152
J. Phys. Chem. C 2022, 126, 7000−7011

h^+ lifetime generated under irradiation.[6] To date, ZnO (E_g = 3.37 eV) and TiO_2 (E_g = 3.20 eV) are both considered promising photocatalysts for environmental remediation[7,8] since they exhibit relatively high photocatalytic activities, as well as for their nontoxicity to biological systems. However, due to the value of their E_g, both of these semiconductors inefficiently use sunlight as they can only be activated by UV light which is a limited fraction (3−5%) of the solar spectrum. Nevertheless, the catalytic efficiency of anatase TiO_2 can be appropriately improved with electronic modifications based on the doping of the semiconductor lattice with metal or nonmetal compounds.[9,10] However, since the first paper of Sato,[11] considerable interest was focused on TiO_2 doping with nonmetal ions, especially with nitrogen. Many papers report that the doping of TiO_2 with nitrogen shows significant catalytic activity in a large variety of chemical reactions performed under visible light irradiation.[12] However, there is still an open debate on how doping with nitrogen promotes photoactivity under visible light. One of the key questions which need to be answered to characterize the properties and behavior of N-doped TiO_2 concerns the location in the lattice and the involvement in photoactivity of the nitrogen species. For understanding the properties of this photocatalytic material, it is important to know if the nitrogen species are primarily interstitial or substitutional, because the behavior of these two species is very different and will affect the material properties accordingly.[13] However, the doping with nitrogen also brings new recombination centers for the photoinduced charge carriers, which results in the quantum efficiency loss caused by the charge pair recombination phenomena.[14] For overcoming this last issue, recently, the use of hybrid photocatalysts has been proposed since the generation of suitable heterojunctions effectively promotes charge carrier separation into different moieties, resulting in a lower recombination probability and higher photoactivity.[15] The construction of a semiconductor heterojunction is based on the presence of two semiconductors[16] (S1 and S2) in which the band potentials are matched to construct an efficient heterostructure. When both photocatalysts are excited by an incident light with sufficient energy to generate electron−hole pairs, if the CB level of S2 is lower than that of S1, electrons in the CB of S1 can be transferred to the CB of S2. On the other hand, if the S2 VB level is lower than that of S1, holes in the S2 VB can be transferred to that of S1. It is argued that, in the heterojunction, an internal electric field at the interface between S1 and S2 is generated, which prevents to some extent the electron−hole recombination phenomena that commonly occur when a single semiconductor is excited.[16]

Additionally, a larger number of electrons on the S2 CB and holes on the S1 VB can, respectively, participate in photoredox reactions to directly or indirectly degrade organic pollutants and thus the photocatalytic reaction can be greatly enhanced.

An example of a heterojunction reported in the literature is that achieved by coupling TiO_2 and ZnO.[17] This type of heterojunction promotes the formation of Zn−O−Ti cross-links, generating oxygen vacancies in TiO_2.[17] The electronic states at the interface of TiO_2 and ZnO are thus modified in such a way that the photogenerated charge carriers are moved away from each other and the lifetime of the electron−hole pair is lengthened.[16]

In conclusion, a photocatalyst composite, which combines the beneficial effects of doping and heterojunctions, could be an ideal catalytic system because the doped catalyst improves the visible light absorption, while the second semiconductor helps to prevent the detrimental recombination phenomena of photogenerated charges. For this reason, the aim of this paper was to perform a study of ZnO/N-doped TiO_2 heterojunctions from an experimental and theoretical point of view. Density functional theory (DFT) calculations were carried out to rationalize theoretically the changes in the band gap energy experimentally observed for N-doped TiO_2 and to define the interface structure and band alignment of ZnO/N-doped TiO_2 heterojunctions. Moreover, the photocatalysts were tested in the UV and visible light driven degradation of atrazine (used as a model colorless pollutant of emerging concern[18−20]), and the results achieved by using scavenger molecules for ROS were used to validate the DFT results and to define a model able to describe the band alignment together with the photogenerated charge-transfer mechanism for ZnO/N-doped TiO_2 heterojunctions.

2. EXPERIMENTAL SECTION

2.1. Materials. Atrazine (2-chloro-4-ethylamino-6-isopropylamino-1,3,5-triazine, analytical standard) was purchased from Sigma-Aldrich. Zinc oxide (ZnO) and titanium dioxide (TiO_2) were supplied by Sigma-Aldrich and Millennium Inorganic Chemicals, respectively. Ammonia aqueous solution at 30 wt %, titanium tetraisopropoxide (97 wt %), and isopropanol (99.5%) were purchased from Sigma-Aldrich.

2.2. Photocatalyst Preparation. Commercial titania (PC50) and zinc oxide were employed as reference materials and used as received. It has been widely reported that doping with nitrogen is an effective method to improve the photocatalytic properties of TiO_2 under visible light.[13] For this reason, to evaluate the effect of nitrogen doping over the photocatalytic activity, different types of photocatalysts were synthesized. First, nitrogen-doped TiO_2 (NdT) photocatalyst was prepared by the sol−gel method, according to the method reported in refs 11, 21. In detail, 100 mL of ammonia aqueous solution was added dropwise to 25 mL of titanium tetraisopropoxide at 0 °C as the solution was stirred. The reaction involves the formation of a white precipitate that was washed with distilled water and centrifuged. Finally, the obtained precipitate was calcined at 450 °C for 30 min to get an optimized visible photoactive named NdT.[22] Then, ZnO/TiO_2 and ZnO/N-doped TiO_2 photocatalysts were prepared by appropriately mixing two single semiconductors (commercial zinc oxide with NdT or with commercial TiO_2). To obtain photocatalysts with a semiconductor−semiconductor heterojunction, the following steps were taken with different compositions: different amounts of ZnO (0.176 and 0.4285 g) and NdT or TiO_2 (1 g) are added to an aqueous solution (100 mL) of isopropanol (1 M). After this, the solvent was evaporated at 80 °C under continuous stirring.[23] The final samples are named *x*ZNT and *x*ZT, where *x* is the ZnO content (wt %). Commercial titania (PC50) was named "TiO_2" in the whole paper.

2.3. Photocatalyst Characterization Techniques. Different characterization techniques were used to examine the physical and chemical properties of all prepared materials. Specific surface area (S_{BET}) measurements were evaluated from dynamic N_2 adsorption measurement at −196 °C by using a Costech Sorptometer 1042 instrument. Before the analysis, the samples were pretreated at 150 °C for 30 min in He flow. Diffuse reflectance spectra (UV−vis DRS) were measured for evaluating the light absorption properties of the samples and

https://doi.org/10.1021/acs.jpcc.2c00152
J. Phys. Chem. C 2022, 126, 7000−7011

the absorption spectra were obtained using a PerkinElmer spectrophotometer Lambda 35. All spectra were obtained using an 88-sample positioning holder, giving total reflectance relative to a calibrated standard SRS-010-99 (Labsphere Inc., North Sutton, NH, USA). The reflectance data were reported as the $F(R\infty)$ values (KM), from Kubelka−Munk theory, vs wavelength. Band gap values were determined by plotting $(KM^*h\nu)^2$ vs $h\nu$ (eV) in the case of direct transition or by plotting $(KM^*h\nu)^{1/2}$ vs $h\nu$ in the case of indirect transition. Wide-angle X-ray diffraction (WAXD) patterns were obtained on a D8 Bruker diffractometer equipped with a Ni filter and a graphite monochromator, CuKα radiation was employed.

The crystallite average sizes (D) were calculated using the Scherrer equation:

$$D = \frac{0.9\,\lambda}{\beta\cos\theta}$$

where β is the full width at half maximum expressed in radians, λ is the wavelength, and θ is the X-ray diffraction angle. D values were calculated considering the (101) reflex for titania in the anatase phase and the (100) reflex for the ZnO wurtzite phase.

2.4. Photocatalytic Activity Tests under UV and Visible Light. A cylindrical batch photoreactor (ID = 2.6 cm, L_{TOT} = 41 cm, and V_{TOT} = 200 mL) in pyrex material was used for all the photocatalytic tests. UV or visible-LED strips (nominal power: 10 W; provided by LED LightingHut; emission range: 365 or 400−700 nm, respectively; light intensity: 13 or 16 mW/cm^2, respectively) were placed around and in contact with the external body of a photoreactor for total irradiation of the volume of the solution. The volume of the treated solution was 75 mL with an initial concentration of 100 μg/L atrazine and a photocatalyst amount equal to 30 mg. The suspension was maintained under dark conditions for 60 min to reach the adsorption/desorption equilibrium of the pollutants on the photocatalyst surface. After the dark period, the suspension was exposed to a light source for 180 min. To avoid the sedimentation of the catalyst at the bottom of the photoreactor, the reaction suspension was continuously mixed using a peristaltic pump. Moreover, the system was equipped with an air distributor device (Q_{air} = 150 cm^{3}min^{-1} (STP)) to ensure the presence of oxygen in the reaction medium.

At different times, about 2 mL of the suspension was withdrawn from the photoreactor and filtered with a SimplePure filter (CA, porosity 0.22 μm) to remove the catalyst particle. For the analysis of the aqueous solution recovered during the photocatalytic reaction an HPLC UltiMate 3000 Thermo Scientific system (equipped with a DAD detector, quaternary pump, column thermostat, and automatic sample injector with a 100 μL loop) equipped with a reversed-phase Luna 5u C18 column (150 mm × 4.6 mm i.d., pore size 5 μm) (Phenomenex) was used for the analysis of atrazine at 25 °C. The mobile phase consisted of an acetonitrile/water mixture (70/30 v/v). The flow rate, injection volume, and detection wavelength were 1 mL/min, 80 μL, and 221 nm, respectively.

2.5. Computational Details. The reported calculations, relating to the bulk undoped TiO_2 and N-doped TiO_2 (NdT) as well as for ZnO/TiO_2 and ZnO/NdT interfaces, are based on the DFT and have been performed with the Quantum ESPRESSO computer package.[24] The exchange and correlation energy functional expressed in the Perdew−Burke−Ernzerhof generalized gradient approximation[25] has been employed. The spin-polarized Kohn−Sham equations were solved in the plane-wave pseudopotential framework, with the wave function basis set and the Fourier representation of the charge density being limited by kinetic cutoffs of 40 and 250 Ry, respectively. The Ti, Zn, O, and N atoms were described by ultrasoft pseudopotentials.[26] We performed DFT + U (U = 3.9 eV) calculations in order to better describe the electronic structure of TiO_2.[27−30]

For more details related to model building see Section S2 of the Supporting Information.

3. RESULTS AND DISCUSSION

3.1. WAXD and Specific Surface Area Results. Table 1 shows the specific surface area values (S_{BET}) obtained by the BET method for all the photocatalysts. S_{BET} of ZnO was 6 m^2/g and those of TiO_2 and NdT were 44 and 60 m^2/g, respectively. S_{BET} of 15ZT (36 m^2/g) and 15ZNT (45 m^2/g) photocatalysts with a semiconductor−semiconductor heterojunction were lower than both TiO_2 and NdT but higher than ZnO, as expected. Therefore, the higher S_{BET} value of 15ZNT with respect to that of 15ZT is related to the S_{BET} of NdT that is higher than TiO_2.

Table 1. Specific Surface Area Values (S_{BET}), Optical Band Gap Energy (E_{bg}), and Crystallite Size (D) of the Analyzed Photocatalysts[a]

				D (nm)	
sample	S_{BET} (m^2/g)	$E_{bg}(D)$ (eV)	$E_{bg}(I)$ (eV)	anatase	wurtzite
TiO_2	44		3.16	26	
ZnO	6	3.15			24
15ZT	36	3.23	3.22	26.4	24.8
NdT	68		2.9−2.25	16	
15ZNT	45	3.17−2.55	3.17−2.55	16.3	24.3

[a] S_{BET} is the specific surface area; $E_{bg}(D)$ is the optical band gap energy for direct transition; $E_{bg}(I)$ is the optical band gap energy for indirect transition; and D is the crystallite size.

X-ray diffraction patterns (WAXD) of all catalysts are shown in Figure S1 (Section S1 in the Supporting Information). The 15ZNT sample (Figure S1a) presents the WAXD pattern of both NdT (main reflections at 2θ = 25.3° and 48°, typical of titania in the anatase phase)[21] and ZnO (main reflections at 2θ = 31.9°, 34.5°, and 36.3°, typical of the ZnO wurtzite phase),[31] shown in Figure S1b. Likewise, the WAXD spectrum of the 15ZNT sample (Figure S1a) confirms the presence of both ZnO and TiO_2 in wurtzite and anatase phases (Figure S1b), respectively. Moreover, crystallite size (D) for wurtzite and anatase phases in 15ZT and 15ZNT samples (Table 1) are very similar to ZnO, TiO_2, and NdT alone, suggesting that no crystalline modification occurred when the heterojunction is realized by means of the preparation method used in this work.

3.2. UV−Vis DRS Results and Optical Band Gap Energy of TiO_2, NdT, 15ZT, and 15ZNT. The data obtained from UV−vis reflectance spectra of TiO_2 and NdT (shown in Figure S2 of Section S1 in the Supporting Information) were used for evaluating the optical band gap energy for indirect transition (shown in Table 1 and labeled as $E_{bg}(I)$) by plotting $(KM \times h\nu)^{1/2}$ vs $h\nu$ (Figures 1 and S3 of Section S1 for the curves in the range 0−12), since titania in the anatase phase is typically considered as an indirect band gap semiconductor.[32] The $E_{bg}(I)$ for TiO_2 is about 3.16 eV (see the x-axis intercept of the tangent to the blue curve in Figure 1 and Table 1). On

https://doi.org/10.1021/acs.jpcc.2c00152
J. Phys. Chem. C 2022, 126, 7000−7011

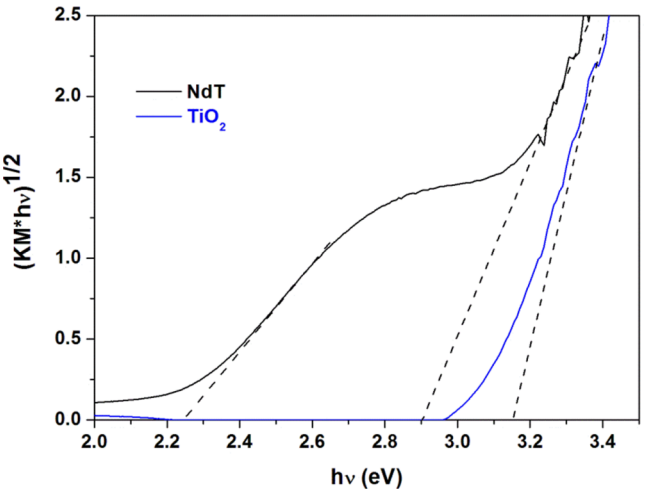

Figure 1. Indirect optical band gap energy calculation of TiO_2 and NdT photocatalysts.

the other hand, from the comparison between NdT and TiO_2, it is evident that the introduction of nitrogen in the TiO_2 lattice slightly affects the absorption edge in the UV region and induces an absorption band in the visible region corresponding to an $E_{bg}(I)$ of about 2.25 eV (see the first *x*-axis intercept of the tangent to the black curve in Figure 1 and Table 1).

In Figure 2 $(KM \times h\nu)^2$ vs $h\nu$ is plotted for 15ZT and 15ZNT and the band gap values for direct transition are shown

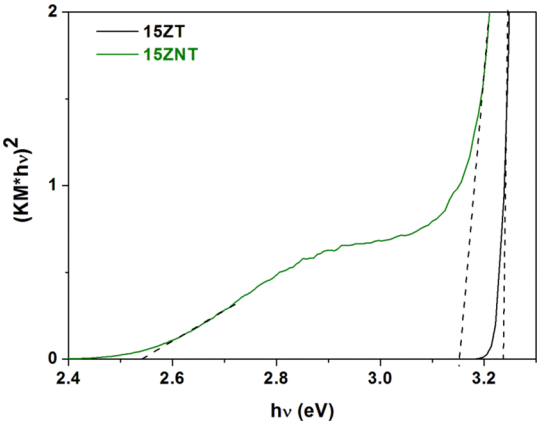

Figure 2. Direct optical band gap energy calculation of 15ZT and 15ZNT photocatalysts.

in Table 1 (labeled as $E_{bg}(D)$) together with the $E_{bg}(D)$ of ZnO obtained from its UV−vis reflectance spectrum (shown in Figure S2 of Section S1 in the Supporting Information). It is important to point out that only the direct transition was considered in the case of bare ZnO, since it is generally considered as a direct band gap semiconductor.[33]

In Figure 3, the curves of $(KM \times h\nu)^{1/2}$ vs $h\nu$ for both 15ZT and 15ZNT are instead shown and the band gap values for indirect transition are also shown in Table 1. It was observed that $E_{bg}(I)$ and $E_{bg}(D)$ values are very similar for both the samples.

However, the oxide combination does not significantly modify the band gap value in the UV region in the case of the ZnO/TiO_2 heterojunction, whereas a slight increase from 2.9 to 3.17 eV in the case of the ZnO/NdT heterojunction was observed. Moreover, the use of different oxide ratios did not

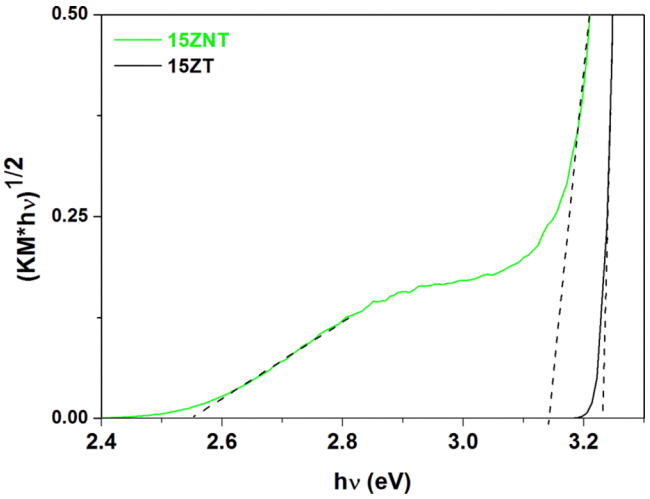

Figure 3. Indirect optical band gap energy calculation of 15ZT and 15ZNT photocatalysts.

have a significant effect over this parameter. On the other hand, from Figures 2 and 3, it is possible to note that the 15ZNT sample presents a shoulder in the visible region of the electromagnetic spectrum (with an absorption edge at 2.55 eV) due to the presence of NdT in the heterojunction.

Based on the results of the experimental characterization, DFT calculations have been performed to gain a deeper understanding of the effect of N-doping on the structural and electronic properties of the NdT system, as well as on the ZnO/NdT heterojunction.

3.3. DFT Calculations of NdT and ZnO/NdT Heterojunctions. *3.3.1. Model and Electronic Structure of Substitutional and Interstitial N-Doping of the Anatase TiO_2 Bulk.* With the aim to understand the possible structural and electronic rearrangements deriving from the presence of nitrogen in the NdT lattice, the substitutional and interstitial nitrogen (N)-doping of the anatase TiO_2 ($ATiO_2$) bulk was investigated by DFT calculations. In the substitutional doped model, the nitrogen atom replaces a tricoordinated oxygen of the optimized $ATiO_2$ bulk (Figure S4 of the Supporting Information), while in the interstitial one, the added N is bonded to a lattice oxygen.[12,34,35] Figure 4A,B shows the substitutional and interstitial N-doping structures. The corresponding band gap obtained from the plot of the projected density of state (PDOS) (Figure 4A′,B′) was compared with that of pure TiO_2 in the anatase phase (see Section S3 of the Supporting Information).

For both NdT systems, the band gap is 2.9 eV as observed for pure TiO_2 (Figure S5) and in agreement with the experimental results shown in Figure 1 and Table 1. Additionally, the presence of N-doping sites generates additional energy levels between the VB and the CB in the TiO_2 electronic structure.

The PDOS plots of the N-doped models indicate the presence of (i) occupied states, lying very close to the VB in the substitutional N-doping and more shifted toward the Fermi level in the interstitial case; (ii) unoccupied states that are higher energy in the gap above the Fermi level (blue peaks and blue levels in Figure 4A′,B′, respectively); and (iii) in the substitutional N-doping, the unpaired electron of N is entirely localized on its 2p orbital, while in the interstitial model it is

https://doi.org/10.1021/acs.jpcc.2c00152
J. Phys. Chem. C 2022, 126, 7000−7011

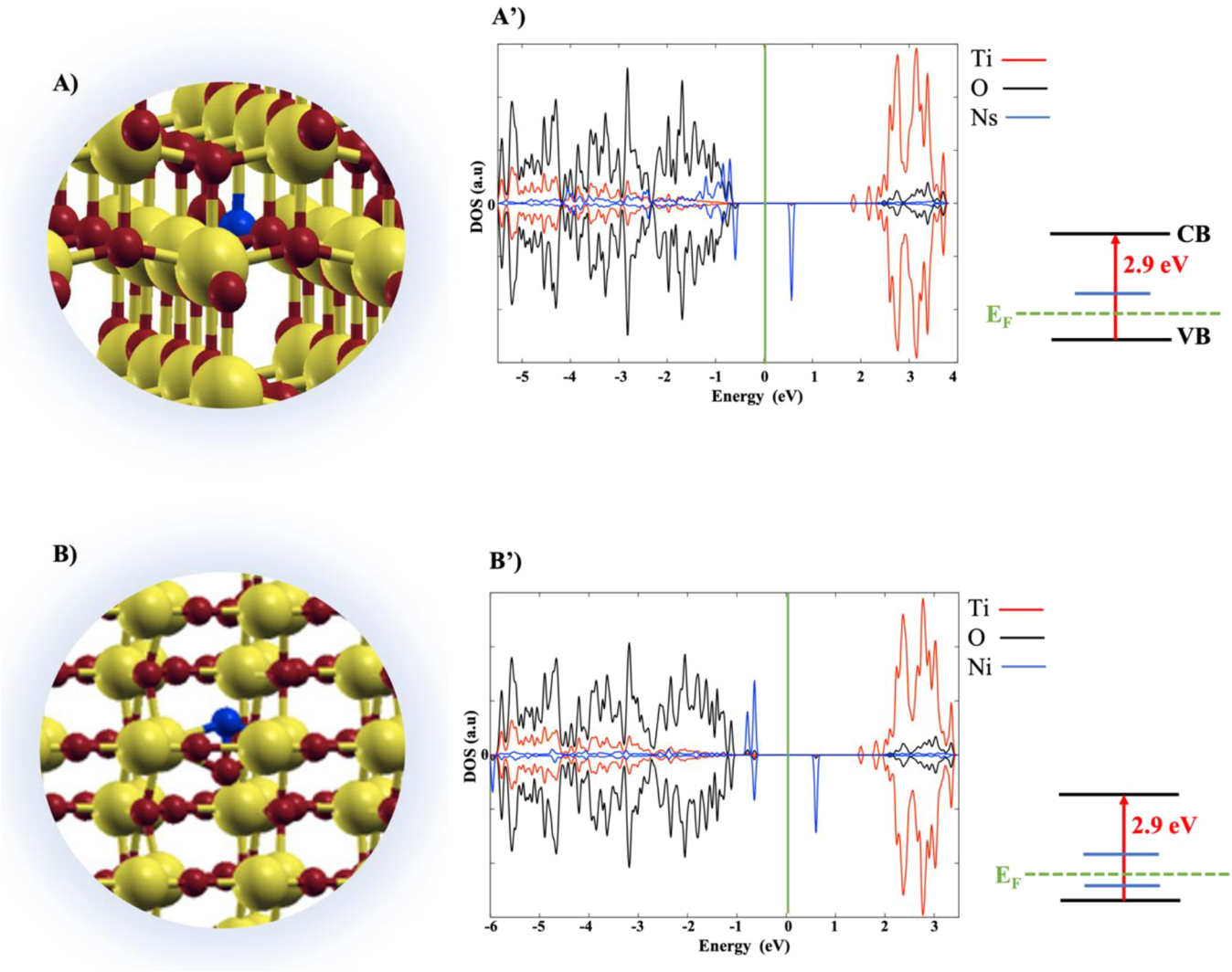

Figure 4. Optimized structures and the PDOS plot of the substitutional and interstitial N-doped anatase bulk (A, A′ and B, B′, respectively). Ti, O, and N atoms are represented as ball and sticks and depicted in yellow, red, and blue, respectively, while the state of Ti, O, and N are represented in red, black, and blue, respectively. On the DOS (a.u.) axis the values above and below 0 a.u. indicate the electrons with spin up and spin down, respectively. The Fermi energy level is represented with a green line at 0 eV.

shared between N and O atoms (see spin density plots in Figure S6).[12,35]

In conclusion, in the interstitial N-doped system, the shift of the occupied states toward higher energy values than those of the VB causes a band gap reduction of about 0.6 eV. Therefore, despite all the possible limitations deriving from the DFT theory, the new computed band gap is 2.3 eV, very close to the value of 2.25 eV obtained for NdT from UV−vis DRS results (Figure 1).

3.3.2. Model and Electronic Structure of the ZnO/NdT Heterojunction. The undoped heterojunction was modeled by employing the most stable (101) anatase TiO_2 and (100) wurtzite (ZnO) phases, as suggested by WAXD results (Figure S1) and in agreement with previous theoretical studies,[36−40] rescaling the lattice parameters of the TiO_2 (101) surface with respect to those of ZnO (100) (Figure S7).

We have limited our study to the effects of N-doping on the TiO_2 (101) portion of the heterojunction in agreement with experiments. Seven different substitutional sites for N-doping of the TiO_2(101) side of the heterojunction have been considered, denoted as $N^{1...7}_{(101)}$, whose structure is shown in Figure 5A.

The most stable substitutional N-doping configurations are found to be the $N^{3}_{(101)}$, $N^{4}_{(101)}$, and $N^{7}_{(101)}$. In order to investigate the effect of the concentration of N-dopant sites on the band offsets of the heterojunction, we have considered three models in which one, two, and three N-doped sites in the TiO_2 supercell are present, respectively. These three N-doped heterojunctions have been defined for clarity $N^{3}_{(101)}$, $N^{3-4}_{(101)}$, and $N^{3-4-7}_{(101)}$.

For interstitial N-doping of the TiO_2 region, we simulated the three possible N-dopant sites suggested by previous theoretical study[12,34,41] and defined $N^{1*}_{(101)}$, $N^{2*}_{(101)}$, and $N^{3*}_{(101)}$ (Figure 5B).

The most stable interstitial N-doping configuration is seen in $N^{1*}_{(101)}$. Also in this case, the effect of the N-dopant concentration on the heterojunction electronic structure has been investigated considering over $N^{1*}_{(101)}$ also two and three interstitial N-doped sites in the TiO_2 portion, indicated with $N^{1*-1*}_{(101)}$ and $N^{1*-1*-1*}_{(101)}$.

https://doi.org/10.1021/acs.jpcc.2c00152
J. Phys. Chem. C 2022, 126, 7000−7011

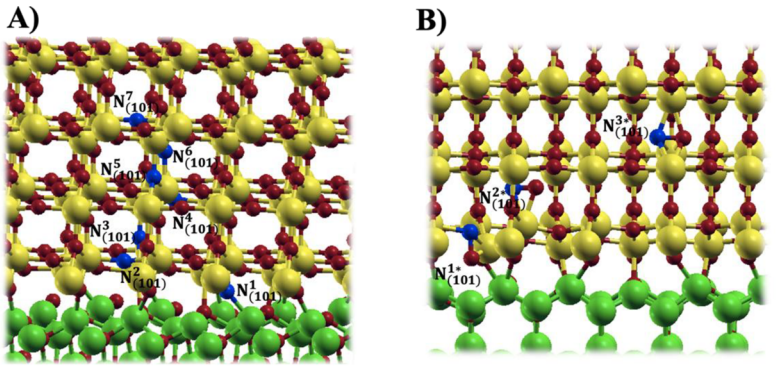

Substitutional N-doped sites	Energy (eV)
$N^1_{(101)}$	0.92
$N^2_{(101)}$	0.09
$N^3_{(101)}$	0.00
$N^4_{(101)}$	0.03
$N^5_{(101)}$	0.05
$N^6_{(101)}$	0.03
$N^7_{(101)}$	0.03

Interstitial N-doped sites	Energy (eV)
$N^{3*}_{(101)}$	0.75
$N^{2*}_{(101)}$	0.64
$N^{1*}_{(101)}$	0.00

Figure 5. Substitutional and interstitial N-doped sites in the $ATiO_2$ (101) region of the heterojunction with the corresponding relative energies in electronvolts. The zero in energy are $N^3_{(101)}$ and $N^{1*}_{(101)}$, which correspond to the most stable substitutional and interstitial N-doped sites, respectively.

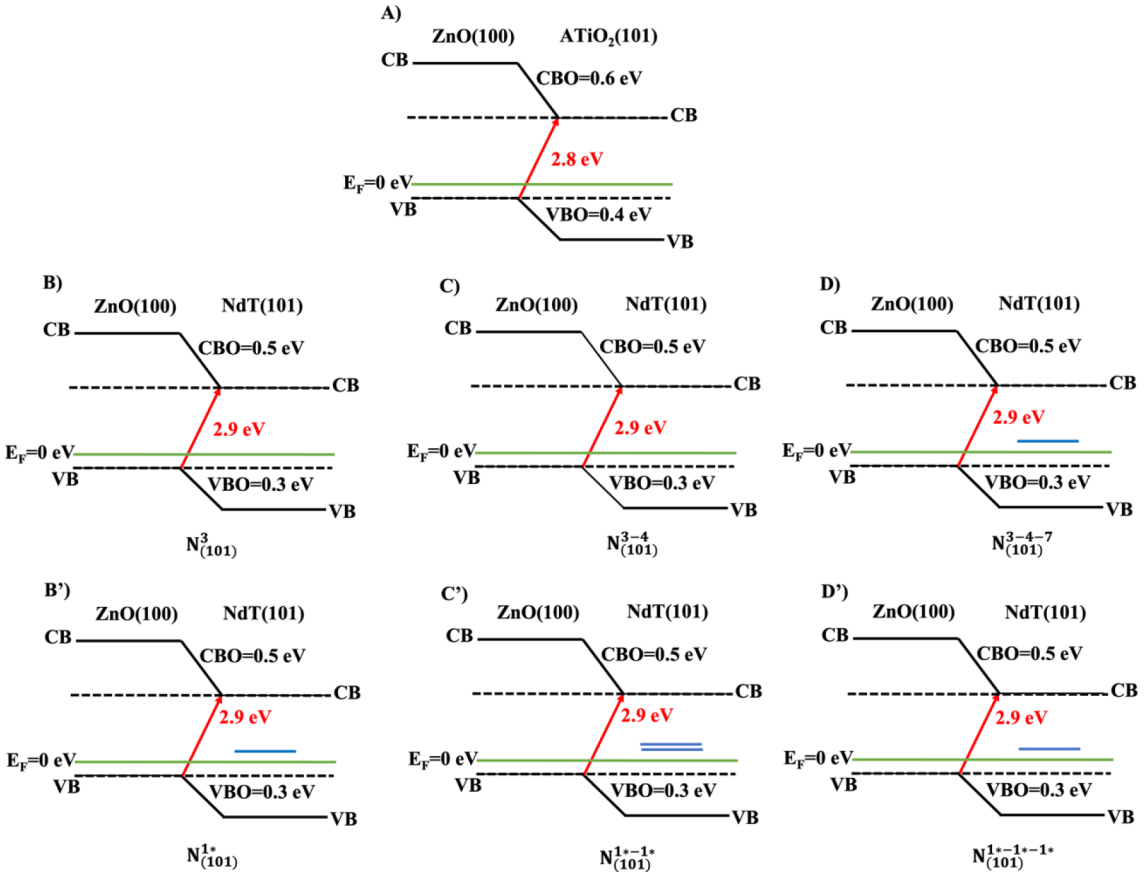

Figure 6. Band alignment of (A) ZnO/TiO_2, substitutional (B–D) and interstitial (B′, C′, and D′) ZnO/NdT heterojunctions.

The relative energy (E, eV) of the substitutional and interstitial N-doped sites in the $ATiO_2$ portion of the heterojunction was computed by using eqs 1 and 2 (see the Supporting Information).

https://doi.org/10.1021/acs.jpcc.2c00152
J. Phys. Chem. C 2022, 126, 7000−7011

The VBO and the CBO of ZnO/TiO_2 and of all ZnO/NdT systems have been defined through eqs 3 and 4 (see the Supporting Information) and are shown in Figure 6.

In the undoped interface, the VBO and the CBO are 0.4 and 0.6 eV, respectively, while the minimal band gap (MBG), calculated using eq 5 (see the Supporting Information), is equal to 2.8 eV (Figure 6A). The computed value of the VBO is in good agreement with that experimentally calculated (0.53 ± 0.07) eV.[39,42,43] For the ZnO/NdT heterojunction, the VBO(CBO) and the minimal band gaps are 0.3(0.5) and 2.9 eV, respectively (Figure 6B–D and B′–D′ for most stable substitutional and interstitial N-doped sites, respectively).

The PDOS plots of the ZnO/TiO_2 (Figure S8) and ZnO/NdT heterojunctions indicate that the presence of substitutional and interstitial N-doped sites generate band gap states above the Fermi level (E_F) (Figures S9 and S10, respectively), which correspond to unoccupied orbitals. It is interesting to note that the substitutional doping generates these higher energy orbitals at high N-dopant concentrations (see blue levels and blue peaks in Figures 6D and S9 relative to the $N^{3-}_{(101)}{}^{4-}{}^{7}$system), while in the case of interstitial doping, these band gap states above the Fermi level (E_F) are already present at low N concentrations (see blue levels and blue peaks in Figures 6B′–D′ and S10). Therefore, the concentration and the position of the N-dopant does not influence the band offset calculations but affect the electronic structure of the heterojunctions, generating additional energy levels between the VB and the CB.

The mixed N-doped heterojunction, defined for clarity $N^{3-}_{(101)}{}^{1}$*, is described in Section S4 of the Supporting Information.

3.4. Photocatalytic Activity Results. Photocatalytic atrazine (ATZ) degradation under UV irradiation was investigated using NdT, ZnO, and 15ZNT samples (Figure 7). The experimental results evidenced that ZnO is much more

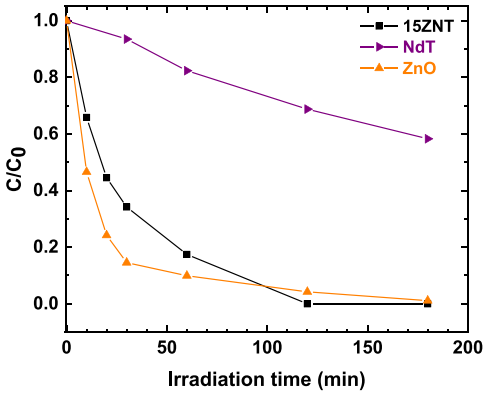

Figure 7. Photocatalytic process driven by UV light for NdT, ZnO, and 15ZNT samples as a function of UV irradiation time.

active than bare NdT, leading to the almost complete ATZ degradation after 180 min of UV irradiation. On the other hand, a lower photocatalytic degradation rate is observed for 15ZNT, which, however, is able to assure complete ATZ degradation in 120 min of UV irradiation time.

Figure 8 shows the photocatalytic results under visible light for the 15ZNT heterojunction in comparison with NdT and ZnO (Figure 8a). It is worthwhile to note that the 15ZNT catalyst evidenced better performance of both NdT and ZnO alone, leading to 24% ATZ degradation after 180 min of visible light irradiation. Since it is well known that bare ZnO is not active under visible light,[44] this is a very surprising result also considering that bare NdT showed a photoactivity lower than 15ZNT. It is possible to argue that the heterojunction between NdT and ZnO realizes a synergistic mechanism which is able to enhance the photocatalytic performance toward the ATZ degradation under visible light. On the other hand, to confirm that the visible light activity is due to the presence of NdT in the heterojunction, an additional photocatalytic test was carried out on 15ZT (ZnO/TiO_2) and compared with the results achieved with the 15ZNT sample (Figure 8b).

Only a negligible degradation is observed for the 15ZT sample, highlighting that the heterojunction between two semiconductors (ZnO and TiO_2) active only under UV light, as expected, is not enough to promote the degradation of the target molecule when the system is irradiated by only visible light.

3.4.1. Role of Reactive Oxygen Species. The key reactive species in photocatalytic degradation of organic pollutants are commonly considered to be •OH and $•O_2^-$. In order to analyze the possible role of such radicals on ATZ photodegradation, by using the 15ZNT photocatalyst, the effects of free radical capture were investigated. The corresponding scavenger probe molecules were: (AI) isopropanol (1 mmol L^{-1}) for •OH and (BQ) benzoquinone (0.5 μmol L^{-1}) for $•O_2^-$. Figure 9 shows the effects of the scavengers for ATZ photodegradation in the presence of UV (Figure 9a) and visible light (Figure 9b). In details, the addition of AI and BQ decreased the photoactivity under UV light (Figure 9a) indicating that •OH and $•O_2^-$ were both reactive species involved in the photocatalytic degradation process. In contrast, based on the experimental data (Figure 9b) obtained under visible light, the total inhibition of photocatalytic activity was achieved in the presence of AI indicating that •OH is the only key reactive species for the degradation of ATZ.

3.5. Possible Mechanism for the Photocatalytic Activity of the ZnO/NdT Heterojunction. Based on the results of the photocatalytic reaction quenching tests (•OH and $•O_2^-$ were found to be both reactive species in ATZ photocatalytic degradation under UV irradiation, while •OH was found to be responsible of the photocatalytic processes under visible irradiation) and DFT calculations (the interface gap resulted in smaller band gap energy than the band gap of the two separate semiconductors, and the presence of the N-dopant generates additional energy levels between the VB and the CB in the TiO_2 electronic structure), a possible mechanism for the activation under UV and visible light of the ZnO/NdT heterojunction was proposed.

For this purpose, the edge position of the CB (E_{CB}) for NdT has been determined considering the Mulliken relationship:[45]

$$E_{CB} = X - E_e - 0.5E_{bg}$$

where X is the absolute electronegativity of TiO_2 (5.81 eV);[23] E_e is the energy of free electrons on the hydrogen scale (ca. 4.5 eV); and E_{bg} is the band gap energy of the NdT determined from DFT calculations (Figure 4).

Therefore, using the E_{bg} and the electronegativity value for TiO_2, it was possible to calculate the E_{VB} and the E_{CB} potentials vs NHE for the ZnO/NdT heterojunction considering the VBO, CBO, and MBG values achieved from DFT (Figure 6). The obtained results are shown in Figure 10.

The results shown in Figure 9a can be well interpreted in the case of a Z-scheme heterojunction (Figure 10a), as also shown

https://doi.org/10.1021/acs.jpcc.2c00152
J. Phys. Chem. C 2022, 126, 7000–7011

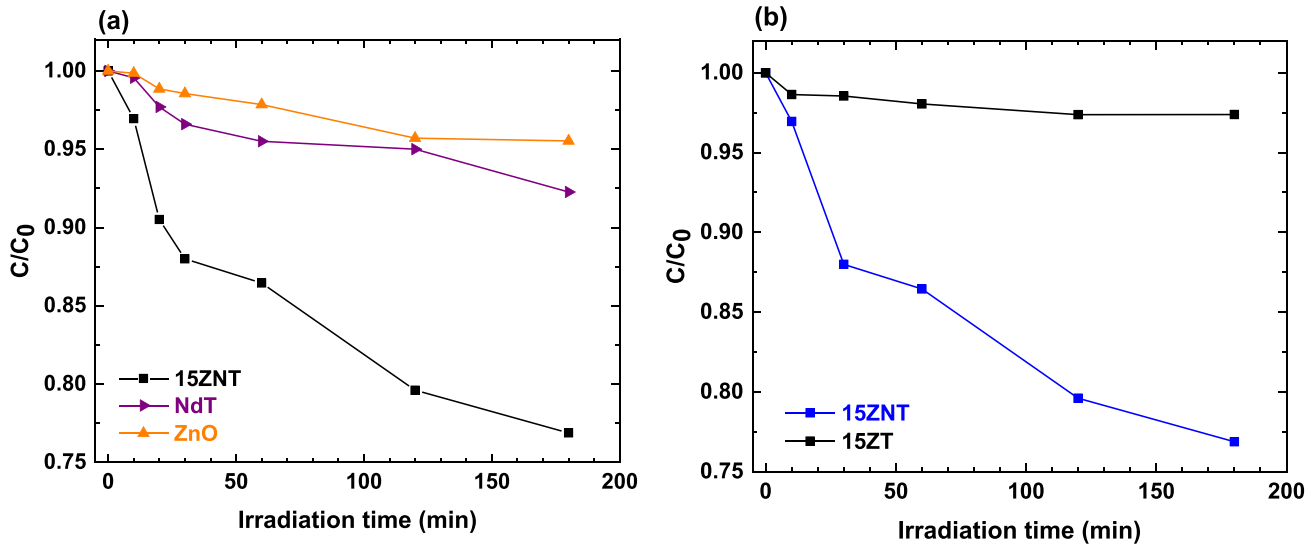

Figure 8. Photocatalytic process driven by visible light for (a) NdT, ZnO, and 15ZNT samples and (b) for 15ZNT and 15ZT as a function of irradiation time.

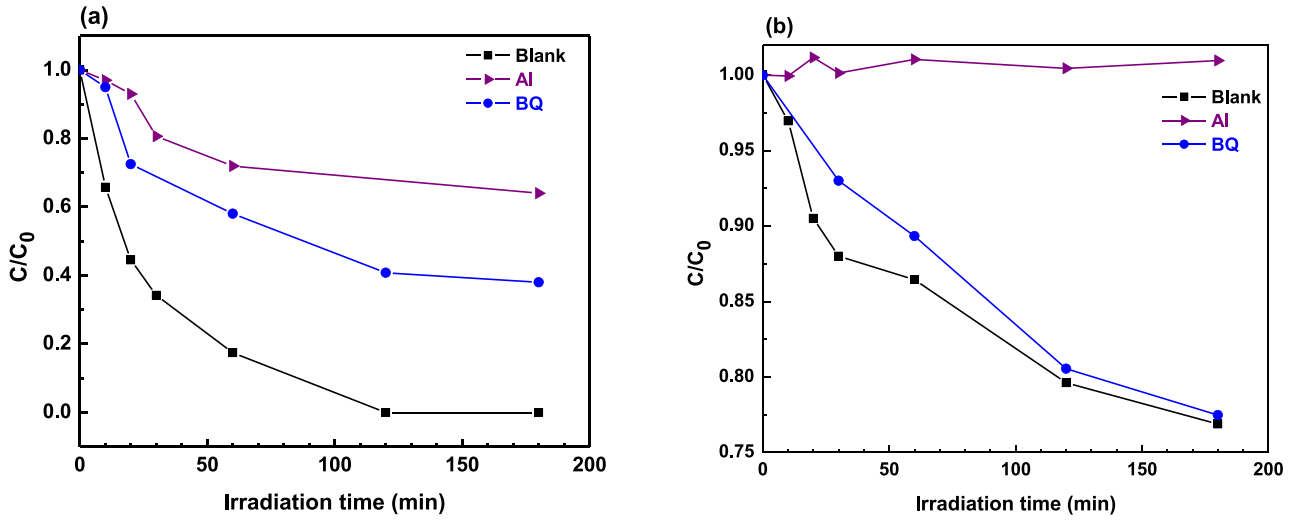

Figure 9. Degradation ATZ by 15ZNT in the presence of radical scavengers under (a) UV and (b) visible light irradiation.

in the literature dealing with the photoactivity of TiO_2 coupled with ZnO under UV light and in which the band alignment of the heterojunction agrees with our DFT results.[46] Specifically, in the presence of UV light, the photogenerated holes are retained in the VB of NdT, whereas, at the interface between the two semiconductors, the electrons migrate from the CB of NdT to the VB of ZnO.[46] This mechanism maintains the photogenerated charge carriers separated in the opposite side of the heterojunction, reducing the e^-/h^+ recombination rate. In this situation, the electrons promoted in the CB of ZnO (having a potential equal to −0.65 eV vs NHE) can reduce oxygen into reactive $\cdot O_2^-$ since the E_{CB} of ZnO is more negative than the standard reduction potential of $O_2/\cdot O_2^-$ (−0.33 eV vs NHE). Meanwhile, the E_{VB} of NdT (+3.05 eV vs NHE) is more positive than that of $\cdot OH/H_2O$ (+2.68 eV vs NHE), and therefore the holes could react with H_2O to form $\cdot OH$. This proposed activation mechanism of photocatalytic processes is in good agreement with the experimental results on the ROS role reported in Figure 9, which showed that $\cdot OH$ and $\cdot O_2^-$ are both responsible of ATZ photocatalytic degradation under UV irradiation (Figure 9a).

In order to confirm the proposed photoinduced charge-transfer mechanism (Figure 10a), the amount of ZnO in the ZnO/N-doped TiO_2 heterojunction was increased up to 30 wt %. The obtained sample (30ZNT) was employed in a test under UV light and its photocatalytic activity was compared with that observed for 15ZNT (Figure 11).

In detail, the behavior of ATZ-relative concentration showed that the 30ZNT sample was more active than 15ZNT, leading to the complete ATZ degradation after 30 min of UV irradiation time, whereas it was about 65% for 15ZNT after the same irradiation time. It is possible to argue that the increased amount of ZnO in the heterojunction is responsible of the generation of more $\cdot O_2^-$ via O_2 reduction with the electrons in the CB of ZnO, validating the photoinduced charge-transfer mechanism under UV irradiation shown in Figure 10a, which is also consistent with a study reporting that the Z-scheme mechanism occurs when TiO_2 is the main component of the ZnO/TiO_2 heterojunction.[47]

Under visible light irradiation, the mechanism is different (Figure 10b). Specifically, the visible light energy could not activate the formation of e^-/h^+ from ZnO. At this range of

https://doi.org/10.1021/acs.jpcc.2c00152
J. Phys. Chem. C 2022, 126, 7000−7011

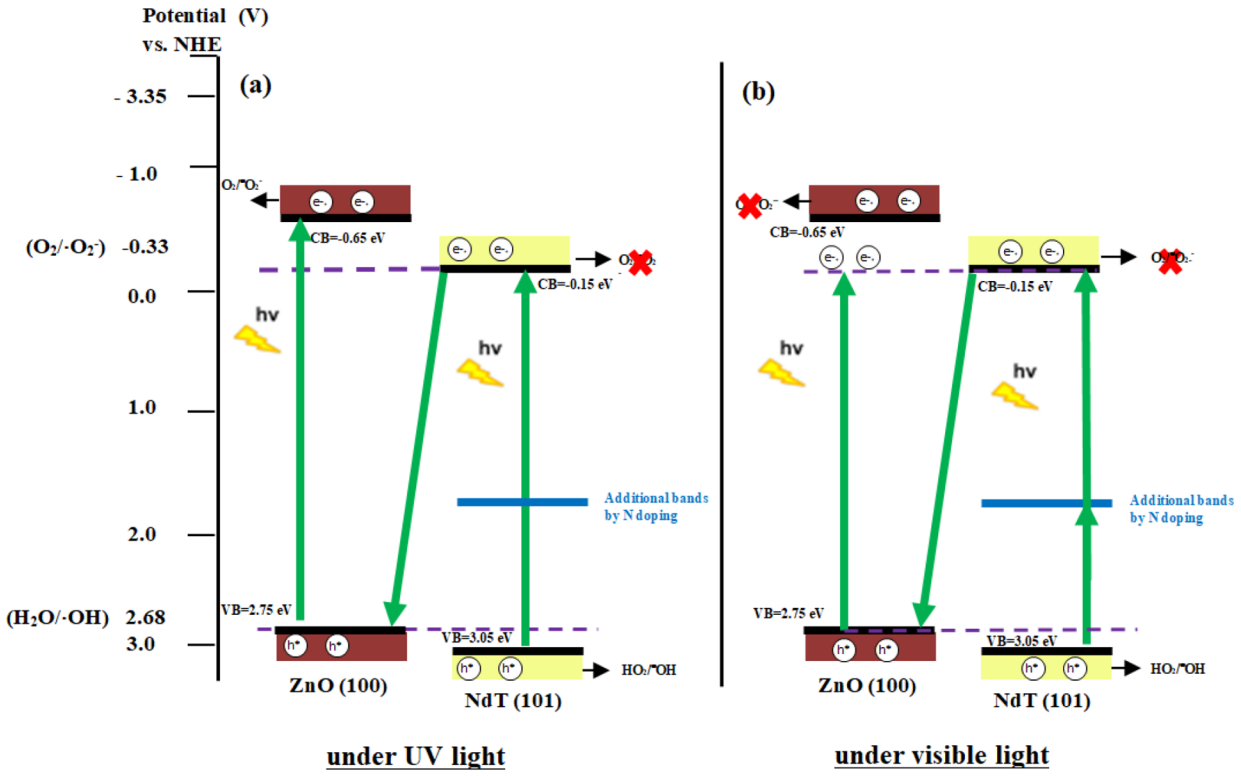

Figure 10. Schematic diagram of ATZ degradation through different schemes of photoinduced charge transfer under (a) UV and (b) visible light irradiation.

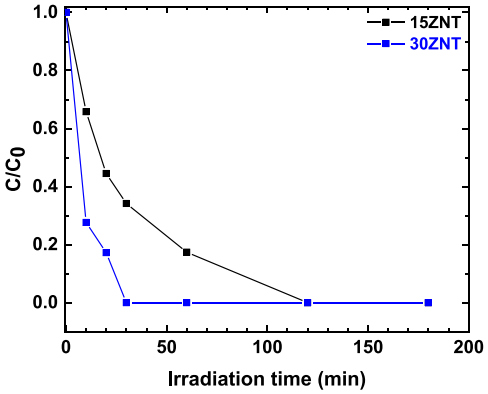

Figure 11. Photocatalytic process driven by UV light for 15ZNT and 30ZNT samples as a function of UV irradiation time.

light irradiation, the photoexcited e^- can be only harvested by NdT due to the DFT-calculated additional energy levels (located at about +2.4 eV) between the VB and the CB in the TiO_2 electronic structure generated by the doping of the TiO_2 lattice with nitrogen. In this way, the e^- generated during irradiation could be transferred on the CB of NdT (−0.15 eV vs NHE) and then on the VB of ZnO (+2.75 eV vs NHE). Simultaneously, since DFT calculations evidenced that the MBG value of the ZnO/NdT heterojunction is equal to 2.9 eV (Figure 6), the electrons can be also promoted from the VB of ZnO to the CB of NdT at the interface but not to the CB of ZnO because of the lower energy associated with visible light. Consequently, since the CB edge of NdT (−0.15 eV vs NHE) is less negative compared to the standard redox potential of $O_2/{\cdot}O_2^-$ (−0.33 eV vs NHE), the generation ${\cdot}O_2^-$ under visible light does not occur. On the other hand, the holes in the VB of NdT are able to react with H_2O promoting the formation of ·OH. However, as far as e^- in the CB is considered, it is possible that it can react with the ATZ byproducts as already reported in the literature.[48] Consequently, the proposed photoinduced charge transfer under visible light (Figure 10b) is validated by the experimental results on the scavenger effect under visible light (Figure 9b), which evidenced that ${\cdot}O_2^-$ is not involved in the ATZ degradation mechanism whereas ·OH plays the most important role in the degradation mechanism of atrazine molecules.

4. CONCLUSIONS

The aim of this paper was to perform a study on the photoactivity of the ZnO/N-doped TiO_2 heterojunction from an experimental and theoretical point of view. To this purpose, DFT calculations are carried out to rationalize theoretically the changes in the band gap energy experimentally observed for N-doped TiO_2 and to define the interface structure and band alignment for the ZnO/N-doped TiO_2 heterojunction, which was tested in the UV and visible light-driven degradation of atrazine. Physical−chemical characterization data revealed the presence of wurtzite ZnO and anatase TiO_2 in the heterojunction. Additionally, the shoulder in the visible region, typically of bare N-doped TiO_2 with band gap energy equal to about 2.5 eV, is preserved in the ZnO/N-doped TiO_2 sample.

DFT calculations (geometries optimization, band alignment, and PDOS) on bulk N-doped TiO_2 in the anatase phase showed that the interstitial N-doped systems induced a band gap reduction of about 0.6 eV with respect to bare TiO_2, evidencing a computed band gap equal to 2.3 eV, in agreement with UV−vis DRS analysis. Additionally, DFT results disclosed that the formation of the heterojunction between ZnO and N-

https://doi.org/10.1021/acs.jpcc.2c00152
J. Phys. Chem. C 2022, 126, 7000−7011

doped TiO_2 gives rise to a smaller band gap than the two single oxide semiconductors and that the presence of substitutional and interstitial N-doped sites generated additional energy levels between the VB and the CB in the TiO_2 electronic structure. Photocatalytic activity results evidenced that ZnO is much more active than bare N-doped TiO_2, leading to the almost complete ATZ degradation after 180 min of UV irradiation. On the other hand, the ZnO/N-doped TiO_2 heterojunction was able to assure the complete atrazine degradation in 120 min of UV irradiation time. Under visible light, the ZnO/N-doped TiO_2 catalyst evidenced better performance of both N-doped TiO_2 and ZnO alone, leading to 24% atrazine degradation after 180 min of irradiation, arguing that the heterojunction between N-doped TiO_2 and ZnO realizes a synergistic mechanism able to enhance the photocatalytic performance toward atrazine degradation. Additionally, the photocatalytic results achieved by using scavenger molecules for ROS evidenced that ·OH and $\cdot O_2^-$ were both responsible of atrazine photocatalytic degradation under UV irradiation, while ·OH was found to be the only reactive species involved in the photocatalytic processes under visible irradiation.

Based on such results and DFT calculations, a model able to describe the band alignment together with the photogenerated charge-transfer mechanism for the ZnO/N-doped TiO_2 heterojunction was proposed, showing that a Z-scheme heterojunction is formed between ZnO and N-doped TiO_2. The formation of the Z-scheme heterojunction facilitates the transport of photogenerated electrons at the interface between the two semiconductors, reducing the e^-/h^+ recombination rate and improving the photocatalytic performance.

■ ASSOCIATED CONTENT

Supporting Information

The Supporting Information is available free of charge at https://pubs.acs.org/doi/10.1021/acs.jpcc.2c00152.

X-ray diffraction patterns of 15ZT, 15ZNT, ZnO, NdT, and TiO_2; UV−vis reflectance spectra for TiO_2, ZnO, 15ZT, NdT, ZnO, and 15ZNT; $(KM^*h\nu)^{1/2}$ (in the range 0−12) vs $h\nu$ for indirect transition (Section S1); theoretical models and methods (Section S2); optimized structure of the undoped anatase bulk; the PDOS plot of the pure anatase bulk; the spin density plot for the substitutional and interstitial N-doped anatase bulk; the optimized structure of the ZnO/TiO_2 heterojunction; graphical representation of $ATiO_2$, ZnO(100)-$ATiO_2$(101) interfaces along with the PDOS; graphical representation of the substitutional N-doped heterojunction; and graphical representation of the interstitial N-doped heterojunction (Sections S3); and the mixed N-doped heterojunction and band alignment and graphical representation of the mixed N-doped heterojunction (Section S4) (PDF)

■ AUTHOR INFORMATION

Corresponding Authors

Lucia Caporaso − *Department of Chemistry and Biology "A. Zambelli", INSTM Research Unit, University of Salerno, 84084 Fisciano, SA, Italy;* orcid.org/0000-0001-6623-3315; Email: lcaporaso@unisa.it

Vincenzo Venditto − *Department of Chemistry and Biology "A. Zambelli", INSTM Research Unit, University of Salerno, 84084 Fisciano, SA, Italy;* orcid.org/0000-0003-4025-6310; Email: vvenditto@unisa.it

Authors

Wanda Navarra − *Department of Chemistry and Biology "A. Zambelli", INSTM Research Unit, University of Salerno, 84084 Fisciano, SA, Italy*

Ida Ritacco − *Department of Chemistry and Biology "A. Zambelli", INSTM Research Unit, University of Salerno, 84084 Fisciano, SA, Italy;* orcid.org/0000-0001-7637-7355

Olga Sacco − *Department of Chemistry and Biology "A. Zambelli", INSTM Research Unit, University of Salerno, 84084 Fisciano, SA, Italy*

Matteo Farnesi Camellone − *CNR-IOM, Consiglio Nazionale delle Ricerche − Istituto Officina dei Materiali, 34136 Trieste, Italy;* orcid.org/0000-0001-9180-0115

Vincenzo Vaiano − *Department of Industrial Engineering, INSTM Research Unit, University of Salerno, 84084 Fisciano, SA, Italy*

Complete contact information is available at: https://pubs.acs.org/10.1021/acs.jpcc.2c00152

Author Contributions

‖W.N., I.R., and O.S. contributed equally to this paper.

Notes

The authors declare no competing financial interest.

■ ACKNOWLEDGMENTS

This research was financially supported by the University of Salerno (FARB19-"Fotocatalizzatori innovativi per l'ambiente e l'energia").

■ REFERENCES

(1) Botta, A.; Costabile, C.; Venditto, V.; Pragliola, S.; Liguori, R.; Rubino, A.; Alberga, D.; Savarese, M.; Adamo, C. Optoeletronic Properties of Poly(N-Alkenyl-Carbazole)s Driven by Polymer Stereoregularity. *J. Polym. Sci., Part A: Polym. Chem.* **2018**, *56*, 242−251.

(2) Botta, A.; Pragliola, S.; Vincenzo, V.; Rubino, A.; Aprano, S.; De Girolamo Del Mauro, A.; Maglione, M.; Minarini, C. Highly Isotactic Poly(N-Pentenyl-Carbazole): A Challenging Polymer for Optoelectronic Applications. *AIP Conf. Proc.* **2014**, *1599*, 493−497.

(3) Baxter, J.; Bian, Z.; Chen, G.; Danielson, D.; Dresselhaus, M. S.; Fedorov, A. G.; Fisher, T. S.; Jones, C. W.; Maginn, E.; Kortshagen, U.; Manthiram, A.; Nozik, A.; Rolison, D. R.; Sands, T.; Shi, L.; Sholl, D.; Wu, Y. Nanoscale Design to Enable the Revolution in Renewable Energy. *Energy Environ. Sci.* **2009**, *2*, 559−588.

(4) Wang, W.; Dai, R.; Zhang, L.; Wu, Q.; Wang, X.; Zhang, S.; Shao, T.; Zhang, F.; Yan, J.; Zhang, W. Experimental and DFT Investigation on the Different Effects of Er^{3+}- and Ag^+-Doped BiOBr Microspheres in Enhancing Photocatalytic Activity under Visible Light Irradiation. *J. Mater. Sci.* **2020**, *55*, 11226−11240.

(5) Pham, T.-D.; Lee, B.-K.; Pham-Cong, D. Advanced Removal of Toluene in Aerosol by Adsorption and Photocatalytic Degradation of Silver-Doped TiO_2/PU under Visible Light Irradiation. *RSC Adv.* **2016**, *6*, 25346−25358.

(6) Wong, K. T.; Kim, S. C.; Yun, K.; Choong, C. E.; Nah, I. W.; Jeon, B.-H.; Yoon, Y.; Jang, M. Understanding the Potential Band Position and e−/h+ Separation Lifetime for Z-Scheme and Type-II Heterojunction Mechanisms for Effective Micropollutant Mineralization: Comparative Experimental and DFT Studies. *Appl. Catal., B* **2020**, *273*, No. 119034.

(7) Franco, P.; Navarra, W.; Sacco, O.; De Marco, I.; Mancuso, A.; Vaiano, V.; Venditto, V. Photocatalytic Degradation of Atrazine under Visible Light Using Gd-Doped ZnO Prepared by Supercritical

Antisolvent Precipitation Route. *Catal. Today* **2021**, DOI: 10.1016/j.cattod.2021.09.025.
(8) Mancuso, A.; Navarra, W.; Sacco, O.; Pragliola, S.; Vaiano, V.; Venditto, V. Photocatalytic Degradation of Thiacloprid Using Tri-Doped TiO_2 Photocatalysts: A Preliminary Comparative Study. *Catalysts* **2021**, *11*, 927.
(9) Khairy, M.; Zakaria, W. Effect of Metal-Doping of TiO_2 Nanoparticles on Their Photocatalytic Activities toward Removal of Organic Dyes. *Egypt. J. Pet.* **2014**, *23*, 419−426.
(10) Etacheri, V.; Di Valentin, C.; Schneider, J.; Bahnemann, D.; Pillai, S. C. Visible-Light Activation of TiO2 Photocatalysts: Advances in Theory and Experiments. *J. Photochem. Photobiol., C* **2015**, *25*, 1−29.
(11) Sato, S. Photocatalytic Activity of NOx-Doped TiO2 in the Visible Light Region. *Chem. Phys. Lett.* **1986**, *123*, 126−128.
(12) Di Valentin, C.; Finazzi, E.; Pacchioni, G.; Selloni, A.; Livraghi, S.; Paganini, M. C.; Giamello, E. N-Doped TiO_2: Theory and Experiment. *Chem. Phys.* **2007**, *339*, 44−56.
(13) Asahi, R.; Morikawa, T.; Ohwaki, T.; Aoki, K.; Taga, Y. Visible-Light Photocatalysis in Nitrogen-Doped Titanium Oxides. *Science* **2001**, *293*, 269−271.
(14) Naldoni, A.; Allieta, M.; Santangelo, S.; Marelli, M.; Fabbri, F.; Cappelli, S.; Bianchi, C. L.; Psaro, R.; Dal Santo, V. Effect of Nature and Location of Defects on Bandgap Narrowing in Black TiO_2 Nanoparticles. *J. Am. Chem. Soc.* **2012**, *134*, 7600−7603.
(15) He, X.; Kai, T.; Ding, P. Heterojunction Photocatalysts for Degradation of the Tetracycline Antibiotic: A Review. *Environ. Chem. Lett.* **2021**, *19*, 4563−4601.
(16) Wang, H.; Zhang, L.; Chen, Z.; Hu, J.; Li, S.; Wang, Z.; Liu, J.; Wang, X. Semiconductor Heterojunction Photocatalysts: Design, Construction, and Photocatalytic Performances. *Chem. Soc. Rev.* **2014**, *43*, 5234−5244.
(17) Huerta-Aguilar, C. A.; Palos-Barba, V.; Thangarasu, P.; Koodali, R. T. Visible Light Driven Photo-Degradation of Congo Red by TiO_2ZnO/Ag: DFT Approach on Synergetic Effect on Band Gap Energy. *Chemosphere* **2018**, *213*, 481−497.
(18) Hallé, C.; Huck, P. M.; Peldszus, S. Emerging Contaminant Removal by Biofiltration: Temperature, Concentration, and EBCT Impacts. *J. AWWA* **2015**, *107*, E364−E379.
(19) Xu, C.; Zhang, J.; Bi, X.; Xu, Z.; He, Y.; Gin, K. Y.-H. Developing an Integrated 3D-Hydrodynamic and Emerging Contaminant Model for Assessing Water Quality in a Yangtze Estuary Reservoir. *Chemosphere* **2017**, *188*, 218−230.
(20) Khan, J. A.; He, X.; Khan, H. M.; Shah, N. S.; Dionysiou, D. D. Oxidative Degradation of Atrazine in Aqueous Solution by UV/H_2O_2/Fe^{2+}, UV/$S_2O_8^{2-}$/Fe^{2+} and UV/HSO_5^-/Fe^{2+} Processes: A Comparative Study. *Chem. Eng. J.* **2013**, *218*, 376−383.
(21) Sacco, O.; Stoller, M.; Vaiano, V.; Ciambelli, P.; Chianese, A.; Sannino, D. Photocatalytic Degradation of Organic Dyes under Visible Light on N-Doped Photocatalysts. *Int. J. Photoenergy* **2012**, *2012*, 626759.
(22) Rizzo, L.; Sannino, D.; Vaiano, V.; Sacco, O.; Scarpa, A.; Pietrogiacomi, D. Effect of Solar Simulated N-Doped TiO_2 Photocatalysis on the Inactivation and Antibiotic Resistance of an E. Coli Strain in Biologically Treated Urban Wastewater. *Appl. Catal., B* **2014**, *144*, 369−378.
(23) Sacco, O.; Murcia, J. J.; Lara, A. E.; Hernández-Laverde, M.; Rojas, H.; Navío, J. A.; Hidalgo, M. C.; Vaiano, V. Pt−TiO_2−Nb_2O_5 Heterojunction as Effective Photocatalyst for the Degradation of Diclofenac and Ketoprofen. *Mater. Sci. Semicond. Process.* **2020**, *107*, No. 104839.
(24) Giannozzi, P.; Andreussi, O.; Brumme, T.; Bunau, O.; Buongiorno Nardelli, M.; Calandra, M.; Car, R.; Cavazzoni, C.; Ceresoli, D.; Cococcioni, M.; Colonna, N.; Carnimeo, I.; Dal Corso, A.; de Gironcoli, S.; Delugas, P.; DiStasio, R. A.; Ferretti, A.; Floris, A.; Fratesi, G.; Fugallo, G.; Gebauer, R.; Gerstmann, U.; Giustino, F.; Gorni, T.; Jia, J.; Kawamura, M.; Ko, H.-Y.; Kokalj, A.; Küçükbenli, E.; Lazzeri, M.; Marsili, M.; Marzari, N.; Mauri, F.; Nguyen, N. L.; Nguyen, H.-V.; Otero-de-la-Roza, A.; Paulatto, L.; Poncé, S.; Rocca, D.; Sabatini, R.; Santra, B.; Schlipf, M.; Seitsonen, A. P.; Smogunov, A.; Timrov, I.; Thonhauser, T.; Umari, P.; Vast, N.; Wu, X.; Baroni, S. Advanced Capabilities for Materials Modelling with Quantum ESPRESSO. *J. Phys.: Condens. Matter* **2017**, *29*, 465901.
(25) Perdew, J. P.; Burke, K.; Ernzerhof, M. Generalized Gradient Approximation Made Simple. *Phys. Rev. Lett.* **1996**, *77*, 3865−3868.
(26) Vanderbilt, D. Soft Self-Consistent Pseudopotentials in a Generalized Eigenvalue Formalism. *Phys. Rev. B* **1990**, *41*, 7892−7895.
(27) Cococcioni, M.; de Gironcoli, S. Linear Response Approach to the Calculation of the Effective Interaction Parameters in the LDA+U Method. *Phys. Rev. B* **2005**, *71*, No. 035105.
(28) Setvin, M.; Franchini, C.; Hao, X.; Schmid, M.; Janotti, A.; Kaltak, M.; Van de Walle, C. G.; Kresse, G.; Diebold, U. Direct View at Excess Electrons in TiO2 Rutile and Anatase. *Phys. Rev. Lett.* **2014**, *113*, No. 086402.
(29) Kowalski, P. M.; Camellone, M. F.; Nair, N. N.; Meyer, B.; Marx, D. Charge Localization Dynamics Induced by Oxygen Vacancies on the TiO_2 (110) Surface. *Phys. Rev. Lett.* **2010**, *105*, No. 146405.
(30) Setvin, M.; Shi, X.; Hulva, J.; Simschitz, T.; Parkinson, G. S.; Schmid, M.; Di Valentin, C.; Selloni, A.; Diebold, U. Methanol on Anatase TiO_2 (101): Mechanistic Insights into Photocatalysis. *ACS Catal.* **2017**, *7*, 7081−7091.
(31) Lee, K. M.; Lai, C. W.; Ngai, K. S.; Juan, J. C. Recent Developments of Zinc Oxide Based Photocatalyst in Water Treatment Technology: A Review. *Water Res.* **2016**, *88*, 428−448.
(32) Zhang, J.; Zhou, P.; Liu, J.; Yu, J. New Understanding of the Difference of Photocatalytic Activity among Anatase, Rutile and Brookite TiO_2. *Phys. Chem. Chem. Phys.* **2014**, *16*, 20382−20386.
(33) Kamarulzaman, N.; Kasim, M. F.; Chayed, N. F. Elucidation of the Highest Valence Band and Lowest Conduction Band Shifts Using XPS for ZnO and $Zn_{0.99}Cu_{0.01}O$ Band Gap Changes. *Results Phys.* **2016**, *6*, 217−230.
(34) Tsetseris, L. Stability and Dynamics of Carbon and Nitrogen Dopants in Anatase TiO_2: A Density Functional Theory Study. *Phys. Rev. B* **2010**, *81*, No. 165205.
(35) Yang, H.; Li, G.; An, T.; Gao, Y.; Fu, J. Photocatalytic Degradation Kinetics and Mechanism of Environmental Pharmaceuticals in Aqueous Suspension of TiO_2: A Case of Sulfa Drugs. *Catal. Today* 2010, *153* (3−4), 200−207, DOI: 10.1016/j.cattod.2010.02.068.
(36) Di Liberto, G.; Tosoni, S.; Pacchioni, G. Nitrogen Doping in Coexposed (001)−(101) Anatase TiO2 Surfaces: A DFT Study. *Phys. Chem. Chem. Phys.* **2019**, *21*, 21497−21505.
(37) Özgür, Ü.; Alivov, Y. I.; Liu, C.; Teke, A.; Reshchikov, M. A.; Doğan, S.; Avrutin, V.; Cho, S.-J.; Morkoç, H. A Comprehensive Review of ZnO Materials and Devices. *J. Appl. Phys.* **2005**, *98*, No. 041301.
(38) Lazzeri, M.; Vittadini, A.; Selloni, A. Structure and Energetics of Stoichiometric TiO_2 Anatase Surfaces. *Phys. Rev. B* **2001**, *63*, No. 155409.
(39) Haffad, S.; Korir Kiprono, K. Interfacial Structure and Electronic Properties of TiO_2/ZnO/TiO_2 for Photocatalytic and Photovoltaic Applications: A Theoretical Study. *Surf. Sci.* **2019**, *686*, 10−16.
(40) Fang, D. Q.; Zhang, S. L. Theoretical Prediction of the Band Offsets at the ZnO/Anatase TiO_2 and GaN/ZnO Heterojunctions Using the Self-Consistent Ab Initio DFT/GGA-1/2 Method. *J. Chem. Phys.* **2016**, *144*, No. 014704.
(41) Livraghi, S.; Paganini, M. C.; Giamello, E.; Selloni, A.; Di Valentin, C.; Pacchioni, G. Origin of Photoactivity of Nitrogen-Doped Titanium Dioxide under Visible Light. *J. Am. Chem. Soc.* **2006**, *128*, 15666−15671.
(42) Wang, J.; Liu, X.-L.; Yang, A.-L.; Zheng, G.-L.; Yang, S.-Y.; Wei, H.-Y.; Zhu, Q.-S.; Wang, Z.-G. Measurement of Wurtzite ZnO/Rutile TiO_2 Heterojunction Band Offsets by x-Ray Photoelectron Spectroscopy. *Appl. Phys. A: Mater. Sci. Process.* **2011**, *103*, 1099−1103.

(43) Scanlon, D. O.; Dunnill, C. W.; Buckeridge, J.; Shevlin, S. A.; Logsdail, A. J.; Woodley, S. M.; Catlow, C. R. A.; Powell, M. J.; Palgrave, R. G.; Parkin, I. P.; Watson, G. W.; Keal, T. W.; Sherwood, P.; Walsh, A.; Sokol, A. A. Band Alignment of Rutile and Anatase TiO2. *Nat. Mater.* **2013**, *12*, 798−801.
(44) Liu, Y.; Wei, S.; Gao, W. Ag/ZnO Heterostructures and Their Photocatalytic Activity under Visible Light: Effect of Reducing Medium. *J. Hazard. Mater.* **2015**, *287*, 59−68.
(45) Pan, G.; Xuejun, Z.; Wenfang, Z.; Jing, W.; Qingju, L. First-Principle Study on Anatase TiO2codoped with Nitrogen and Ytterbium. *J. Semicond.* **2010**, *31*, No. 032001.
(46) Wang, J.; Wang, G.; Wei, X.; Liu, G.; Li, J. ZnO Nanoparticles Implanted in TiO_2 Macrochannels as an Effective Direct Z-Scheme Heterojunction Photocatalyst for Degradation of RhB. *Appl. Surf. Sci.* **2018**, *456*, 666.
(47) Sun, W.; Meng, S.; Zhang, S.; Zheng, X.; Ye, X.; Fu, X.; Chen, S. Insight into the Transfer Mechanisms of Photogenerated Carriers for Heterojunction Photocatalysts with the Analogous Positions of Valence Band and Conduction Band: A Case Study of ZnO/TiO_2. *J. Phys. Chem. C* **2018**, *122*, 15409−15420.
(48) Shah, N. Role of e_{aq}^-, •OH and H• in Radiolytic Degradation of Atrazine: A Kinetic and Mechanistic Approach. *J. Hazard. Mater.* **2014**, *288*, 147−157.

NOTE ADDED AFTER ASAP PUBLICATION

This paper was published ASAP on April 13, 2022 with an error in the caption of Figure 5 and incorrect figure and section references. The corrected version was reposted on April 15, 2022.

https://doi.org/10.1021/acs.jpcc.2c00152
J. Phys. Chem. C 2022, 126, 7000−7011